Published in final edited form as:

Oncogene. 2015 November 26; 34(48): 5869–5878. doi:10.1038/onc.2015.38.

DNA methylation in small cell lung cancer defines distinct disease subtypes and correlates with high expression of *EZH2*

John T. Poirier[1], **Eric E. Gardner**[1], **Nick Connis**[2], **Andre L. Moreira**[1], **Elisa de Stanchina**[1], **Christine L. Hann**[2], and **Charles M. Rudin**[1]

[1]Memorial Sloan Kettering Cancer Center, New York, NY

[2]Sidney Kimmel Comprehensive Cancer Center, Johns Hopkins University, Baltimore MD

Abstract

Small cell lung cancer (SCLC) is an aggressive malignancy characterized by early metastasis, rapid development of resistance to chemotherapy, and genetic instability. This study profiles DNA methylation in SCLC, patient-derived xenografts (PDXs) and cell lines at single nucleotide resolution. DNA methylation patterns of primary samples are distinct from those of cell lines, while PDXs maintain a pattern closely consistent with primary samples. Clustering of DNA methylation and gene expression of primary SCLC revealed distinct disease subtypes among histologically indistinguishable primary patient samples with similar genetic alterations. SCLC is notable for dense clustering of high-level methylation in discrete promoter CpG islands, in a pattern clearly distinct from other lung cancers and strongly correlated with high expression of the E2F target and histone methyltransferase gene *EZH2*. Pharmacologic inhibition of EZH2 in a SCLC PDX markedly inhibited tumor growth.

Keywords

SCLC; epigenetics; methylation; subtypes; EZH2

Introduction

Despite an encouraging decline in lung cancer cases in the United States due in large part to a decreasing prevalence of tobacco use, lung cancer remains the number one cancer killer and is expected to remain so for some time ([1]). Worldwide tobacco use trends point to an increase in lung cancer cases and deaths, particularly in underdeveloped and developing countries ([1, 2]). A subset of lung cancers representing 10–15% of cases is classified as small cell lung cancer (SCLC) ([1, 3]), typified by rapid proliferation, a high rate of early metastasis and extreme lethality; 2/3 of SCLC patients present with metastatic disease and have a 5-

Corresponding author: Charles M. Rudin MD PhD, Memorial Sloan-Kettering Cancer Center, 300 E 66th St., Rm 1203, New York, NY 10065, Phone: 646-888-4527, Fax: 646-888-4676, ; Email: rudinc@mskcc.org

Conflicts of interest: CMR has been a paid consultant regarding cancer drug development for AbbVie, Aveo, Celgene, GlaxoSmithKline, and Merck. JTP has no conflicts of interest.

year survival rate of less than 1% ([4]). The primary standard of care for patients with advanced SCLC has remained the same for over 30 years: a combination the cytotoxic compounds cisplatin and etoposide ([5, 6]).

Two recent comprehensive genomic analyses have identified potential genetic drivers of SCLC ([7, 8]). One interesting outcome from these studies was the identification of hotspot mutations in a number of known chromatin modifiers including the histone acetyl transferase genes *CREBBP* and *EP300*, as well as epigenetic readers such as those encoded by *MLL* and *MLL2*. The effects of these alterations on site-specific DNA methylation and target gene expression have not been defined. A large-scale effort by The Clinical Lung Cancer Genome Project (CLCGP) to develop a genomics-based classification of human lung tumors has proven insightful in correlating specific genetic lesions with lung cancer subtypes and clinical outcomes ([9]). While comprehensive in their genetic analysis, these several studies did not explore the role that epigenetics may play in SCLC etiology and classification.

A primary mechanism of epigenetic regulation of gene expression is DNA methylation. Hypermethylation of CpG islands associated with regulatory elements controlling gene expression can drive secondary recruitment of histone modifications, together leading to stable gene silencing. Several studies have demonstrated that key pathways can be altered in cancers by distinct mechanisms, including mutation, deletion, and DNA methylation ([10–13]). A clearer understanding of the patterns of DNA methylation in SCLC may yield cancer specific biomarkers and help to identify clinically actionable drug targets and pathways through integrated genetic and epigenetic analysis.

Kalari et al. performed a study of DNA methylation patterns in 18 primary SCLC tumors and 5 SCLC cell lines using a target-specific CpG island promoter array ([14]). This study identified DNA methylation peaks in 73 genes specific to SCLC with a significant representation of neuroendocrine-specifying transcription factor genes including *NEUROD1, HAND1, ZNF423, REST*, as well as polycomb genes such as the *HOXD* cluster, but was not able to reliably differentiate tumor from normal lung. This study was further limited by relatively low resolving power of the technique used ([15]), and by the lack of complementary genetic analysis of these samples. The present study sought to substantially extend our understanding of genome-wide DNA methylation in SCLC at single base resolution by performing Illumina Human Methylation 450k analysis on a set of 47 extensively characterized SCLC samples, including 34 fresh frozen primary SCLC tumors with available exome mutation, copy number, and RNA-seq data as well as 6 distinct primary patient-derived xenografts and 7 cell lines (Supplementary Table S1) ([7]). Twenty-four of the primary SCLC tumors had matched normal lung control DNA available for analysis.

Using these complementary data sets, we show that SCLC primary xenografts are epigenetically more similar to primary SCLC than are cell lines, identify differentially methylated regions and individual CpG positions that are correlated with gene expression, and define epigenetically distinct SCLC subtypes among primary patient samples that may have important therapeutic and diagnostic implications. SCLC is a disease that is

characterized by extreme plasticity and cloning capacity consistent with a high level of stemness ([16]). We identified *EZH2*, a member of the PRC2 complex that promotes trimethylation of histone H3 lysine 27 (H3K27me3) and self-renewal as being both highly expressed in SCLC and strongly correlated with overall promoter methylation among many tumor types. Pharmacologic inhibition of EZH2 in LX92, a SCLC PDX, inhibited growth *ex vivo* and *in vivo*, providing preclinical evidence for the utility of this class of epigenetic therapy in SCLC.

Results

DNA Methylation Patterns in models of SCLC

Regions of DNA hypomethylation with high variation in both DNA methylation and gene expression have been reported in many human cancers ([17]). Consistent with these reports, we observed that DNA methylation levels were widely disparate in primary SCLC samples, PDX tumors, and SCLC cell lines compared to normal lung (Supplementary Fig. 1A). In order to estimate DNA methylation variability within each group, we examined the across-sample standard deviations in DNA methylation β-values for each CpG measured. The proportion of highly variable CpGs is low in normal lung and higher in every other group, consistent with high methylation instability in primary samples that is also present in both PDXs and cell lines (Fig. 1A).

We hypothesized that DNA methylation patterns could discriminate between normal lung, primary SCLC, PDXs, and cell lines. Principal component analysis demonstrated that tissue-specific DNA methylation in lung was consistent between samples in contrast to DNA methylation in cancer samples, which was more variable (Fig. 1B). Four of six PDXs clustered with primary SCLC samples, while 7/7 cell lines fell outside of this cluster. All primary SCLC and PDXs could be differentiated from cell lines by just two principal components, which account for almost half of the total variance (Supplementary Figure 1B–C). To further characterize differences among primary SCLC, PDXs, and cell lines, we performed unsupervised hierarchical clustering on inter-sample Spearman correlation coefficients and found that all primary normal samples clustered together, while primary SCLC also clustered together along with 3 classic subtype SCLC PDXs, LX44, LX47, and LX48 (Fig. 1C). All 7 SCLC cell lines as well as 3 variant subtype SCLC PDXs, LX22, LX33 and LX36, clustered together. Variant subtype PDXs may have clustered with SCLC cell lines due to similarity to the variant cell lines H446 and H82; we have previously reported that these cell lines and PDXs share a common neurogenic differentiation program ([18], [19]). This finding is consistent with earlier reports suggesting that PDXs are more similar to primary SCLC based on gene expression than are SCLC cell lines ([20]).

We next compared β-values of primary SCLC, PDXs and cell lines to normal lung and plotted the concordance at the top (CAT) of the ranked probe list obtained from primary SCLC with those obtained from either PDXs or cell lines. While both PDXs and cell lines were >80% concordant with primary SCLC at the top of the ranked probe lists, cell line concordance dropped off rapidly with increasing probe list size while PDXs maintained high concordance with primary SCLC (Fig. 1D) ([21]). Using a significance cutoff based on the CAT plot ($q<1 \times 10^{-6}$) to select significant CpG sites as opposed to a rank order approach,

we confirmed that PDXs maintained 98% concordance with primary SCLC, while cell lines appear to accumulate divergent DNA methylation over time as a result of epigenetic drift and adaptation to cell culture (Fig. 1E–F). Of note, several of these PDX models are of unknown high passage, yet still maintain high concordance with primary tumors. These data suggest that the irreversible changes in gene expression caused by long-term culture *ex vivo* may be driven in part by epigenetic dysregulation not observed when tumors are continuously passaged exclusively in mice.

Differential methylation between SCLC and normal lung

Of the differentially methylated CpG sites (Supplementary Table S2, Supplementary Fig. 2A), the majority of CpGs were hypomethylated in SCLC relative to normal lung; however, the most significant methylation events were predominantly hypermethylated in SCLC (Fig 2A). Concordance of both PDXs and cell lines with primary SCLC was strongly correlated with the fraction of differentially methylated CpGs that were methylated compared to normal lung (Supplementary Fig. 2B). Probes associated with CpG island-containing promoters on the Illumina 450k platform are concentrated within 500 bp of the transcription start site (TSS). Significantly hypermethylated CpGs tend to follow a similar distribution within 500 bp of the TSS, while significantly hypomethylated sites are distributed over a wider range upstream of the TSS (Fig 2B), consistent with reports of general promoter hypomethylation accompanied by cancer-specific hypermethylation proximal to the TSS in bisulfite sequencing data ([22]).

To characterize the significance of promoter methylation on gene expression, the Spearman rank correlation between the β-value at each CpG for every sample and the expression of the gene associated with that promoter was calculated. DNA methylation events that are strongly correlated with alterations in gene expression were calculated among samples where both Illumina 450k and RNA-seq data were available (Supplementary Table S3). Average fold change in gene expression is plotted vs. differential β-value and summarized in Figure 2C. Among significantly hypomethylated CpGs, a distinct bimodal distribution is observed in those associated with high gene expression in contrast to those with apparent silencing, suggesting that demethylation in the gene body is associated with actively transcribed genes. Hypomethylated CpGs associated with high gene expression were more likely to be observed downstream of the TSS in expressed genes than hypomethyated CpGs associated with silenced genes, which predominantly cluster immediately upstream of the TSS (Figure 2D).

Four-hundred and ninety-four ranges comprising 4,033 unique CpGs were identified as significantly differentially methylated using a “bump hunting” approach (Supplementary Table S5) ([23]). The number of probes on the Illumina 450k array limits this general approach to interrogating 27% of probes in 12,502 clusters; however, it is useful for finding regions with consistent tumor-specific differences in local methylation. When comparing the regions identified to those reported in Kalari et al., 32/65 (49%) significant ranges were identified in our data set, while 462 additional unique ranges were detected (Supplementary Figure 2C–D).

One of the most differentially methylated genes in small cell lung cancer in comparison to normal lung that is also strongly correlated with gene expression is the oncogene *BCL2* (Fig. 2E; Supplementary Table S4). This gene is methylated and silenced in normal lung, but shows substantial variability among primary samples and PDXs. We have previously reported that *BCL2* message and its protein product Bcl-2 are more frequently highly expressed in classic subtype than in variant subtype SCLC PDXs. We therefore compared methylation levels of *BCL2* methylation to Bcl-2 protein expression across 3 PDXs of each subtype and found that Bcl-2 was only detectable in classic subtype PDXs, associated with minimal DNA methylation (Figure 2F). Upregulated *BCL2* expression in classic subtype SCLC may be driven primarily by epigenetic mechanisms ([24]).

We also found methylation and inactivation of two tumor suppressor genes, *TCF21* (Supplementary Figure 2E), also identified by Kalari et al., and *RB1* ([25]). *RB1* loss of function is typically by a combination of copy loss and mutation. In cases where these mutations are not fully inactivating, silencing by promoter methylation may play a role in further suppressing *RB1* expression (Supplementary Figure 2F–G).

DNA methylation profiling defines distinct subtypes of SCLC

We hypothesized that disease subtypes characterized by differential DNA methylation and gene expression could be present among the primary SCLC samples in this study. We applied k-means consensus clustering to DNA methylation and gene expression data among primary SCLC samples. Three distinct groups are observed at both the DNA methylation and gene expression levels (Fig. 3A–B). We refer to the three principal methylation clusters identified here as SCLC M1, M2, and SQ-P subgroups and the gene expression clusters as SCLC E1, E2, and SQ-P. Interestingly, extensive model tuning and silhouette analysis indicated the presence of a single, highly stable cluster closely related to a primitive phenotype gene expression cluster previously identified among lung cancers histologically identified as squamous cell lung cancer. This approach that has also been applied to classification of other lung tumor types ([9], [26]). The SQ-P tumors in our tumor set originated from multiple cancer centers and were verified as SCLC by a thoracic pathologist. Other clustering solutions and model tuning approaches were explored, as described in detail in Methods and Materials; however values of k greater than 3 significantly decrease the quality of clustering of samples outside of the SQ-P cluster, while SQ-P cluster membership remains stable up to more than 5 groups (Supplementary Fig. 3). Notably, 6/6 gene expression samples in the SQ-P cluster were concordant with the corresponding DNA methylation cluster, confirming that the methylation patterns observed are clearly tied to gene expression (Figure 3C).

We examined DNA methylation patterns among the CpG sites with the highest variance and found that the cluster identified as SQ-P had what appeared to be overall lower methylation compared the SCLC M1 and M2 subgroups (Figure 4A). We explored the possibility that CpG probe intensities could be affected in the SQ-P subset by tumor purity, a hypothesis that our data did not support. Increased methylation in the SCLC M1 and M2 subtypes can be visualized genome-wide in the density plot shown in Figure 4B and the mean promoter methylation scatter plot in Figure 4C. Consistent hypermethylation is present in M1 and M2

subtypes both genome-wide at single-nucleotide resolution as well as when considering average methylation of promoters. Dilution of the SQ-P subtype by admixture with normal lung tissue or immune infiltrate could be expected to increase the methylation of some promoters while decreasing others; however, DNA methylation was consistently increased in SCLC M1 and M2 subtypes relative to SQ-P. We plotted the number of methylated promoters in each subtype and found that the number of methylated promoters was significantly lower in the SQ-P subtype compared to all other subtypes (Fig. 4D). We further identified which CpG sites were significantly differentially methylated between the SQ-P subtype and SCLC M1 and M2, and among this subset of sites found that the SCLC M1 and M2 subtypes were significantly more frequently methylated (Figure 4E). Significantly differentially methylated CpG sites were also significantly more likely to be found in CpG islands in SCLC M1 and M2 than in the SQ-P subtype (Figure 4F), while the SQ-P displayed a non-significant trend toward increased methylation in LINE repeats (p=.075) that may reflect lack of statistical power due to the relative low coverage of CpG probes in these regions (Fig. 4G). Other groups have identified a CpG island methylator phenotype (CIMP) among various cancer histologies that is often associated with a more aggressive tumor and poorer prognosis ([27–31]). DNA promoter methylation levels in SCLC are among the highest of any tumor type when compared to samples found in TCGA, suggesting that this increased methylation level is biologically significant within the spectrum of human cancer (Figure 4H).

Interestingly, the hallmark SCLC genetic lesions including *TP53* mutation and *RB1* inactivation are present in all subtypes (Figure 5A). We have previously reported that expression of two genes, *NEUROD1* and *ASCL1*, can accurately predict classic vs. variant subtype SCLC cell lines and PDXs ([18]). Differential expression analysis between SCLC E1 and E2 gene expression subgroups demonstrated that these genes follow a similar pattern in primary SCLC samples (Figure 5B). *NEUROD1* expression was high and *ASCL1* was low in the E1 subtype, while the converse was true in the SCLC E2 subtype (Fig. 5; Supplementary Table S6).

EZH2 expression is high in SCLC and correlates with high promoter methylation among cancers in TCGA

We also examined the genes that were highly expressed among all SCLC subtypes relative to normal lung for candidates that could account for the high levels of promoter methylation in SCLC. The chromatin modifier *EZH2* was among the most significantly overexpressed genes in SCLC, expressed >12-fold higher than in normal lung (Fig 6A; Supplementary Table S7). EZH2, a histone methyltransferase component of the PRC2 complex, has been implicated in dysregulation of DNA methylation in cancer through its effects on histone methylation, particularly histone H3 lysine 27 tri-methylation (H3K27me3) ([32]). *EZH2* is a known target of E2F, which is activated in SCLC by gene copy loss and loss of function mutations in *RB1*, the gene encoding the E2F repressor pRB ([33]).

In addition to the high expression observed in SCLC compared to normal lung, we observed a significant correlation between median *EZH2* gene expression and the number of methylated promoters in a given cancer type using data from TCGA (Fig 6B). Overall,

EZH2 expression in SCLC is greater than or comparable to that of any of tumor type represented in either TCGA for primary tumors or the Cancer Cell Line Encyclopedia (CCLE) for cell lines (Fig 6C). High-level *EZH2* gene expression associated with increased methylation in CpG island-containing promoters is a common feature of SCLC.

We next asked whether EZH1 and EZH2 protein expression was detectable in a panel of 17 SCLC PDXs by Western blot (Figure 7A). Neither protein was universally expressed; however, EZH2 expression was detectable in 15/17 SCLC PDXs (88%). We reasoned based on these data that EZH2 could be of interest as a druggable target in SCLC. We therefore treated *ex vivo* cultures of the LX92 PDX with three EZH2 inhibitors: EPZ-5687, GSK343, and UNC1999 over a period of 7 days and measured cell viability by resazurin conversion over time (Figure 7B). All three compounds significantly inhibited viability *ex vivo*. In order to assess the extent of EZH2 inhibition, we performed Western blots for EZH1, EZH2, H3K27me2 and H3K27me3 (Figure 7C). While all three inhibitors decreased levels of H3K27me3, only EPZ-5687 was able to profoundly decrease H3K27me2 levels, suggesting that this compound is a more potent inhibitor of EZH2 at the doses used.

EPZ-6438 is a more potent and bioavailable derivative of EPZ-5687 for *in vivo* use. We assessed the efficacy of EPZ-5687 in the LX92 SCLC PDX *in vivo*. EPZ-5687 was well tolerated (Supplementary Figure S4) and demonstrated remarkable efficacy at 100 mg/kg either QD or BID (Figure 7D).. Tumors were collected on day 43 for pharmacodynamic analysis. Protein lysates from tumors were pooled based on treatment group and degree of tumor growth inhibition (TGI). EZH1 levels were decreased in all EPZ-5687 treatment groups. Interestingly, the best responding tumors in the BID group showed decreased levels of EZH2 and significant inhibition of both H3K27 di- and trimethylation, demonstrating that antitumor efficacy is consistent with target inhibition (Figure 7E).

Discussion

Our understanding of cancer genetics has grown exponentially over the last decade with increasing accessibility to high throughput sequencing technology and plummeting costs for data acquisition. It has been estimated that mutations in fewer than 200 genes drive cancer initiation and progression and that the majority of such oncogenic mutations have been identified ([34]). Many targeted therapies have been developed for these mutations; however, clinically actionable drug targets are disappointingly rare in SCLC. Targeting approaches based on aberrant gene expression may be more tractable in SCLC. One focused proteomic study identified PARP1 and EZH2 as potential actionable targets ([35]). SCLC epigenetics has not been as comprehensively studied as tumor genetics, in part due to the variety of DNA and histone modifications, chromatin modifying enzymes, and the relatively scant tissue available from primary patient samples.

DNA methylation profiles of cells grown in culture tend to be distinct from those of primary tissues with both random and highly consistent changes in methylation being observed ([36], [37]). In contrast, we found that PDX maintain a DNA methylation pattern consistent with primary SCLC even after multiple passages. This supports our earlier gene expression

findings and suggests that epigenetic dysregulation may account in part for the irreversible gene expression changes observed in cell lines and cell line xenografts.

Gene expression and DNA methylation data have begun to shed light on heterogeneity within lung cancer histologies ([10], [26], [38]). SCLC has been historically considered a relatively homogenous disease, supported by near universal genetic alterations in *TP53* and *RB1* and a highly representative mouse model generated through conditional loss of these genes ([39]). Recent large-scale efforts have attempted to improve the classification of lung cancers based on differential spectra of genetic alterations; primitive squamous and large-cell neuroendocrine tumors being among the histologies most difficult to accurately classify. We observed epigenetically distinct subgroups among histologically and genetically similar SCLC cases from multiple institutions and geographic cohorts that may represent clinically important populations. These subgroups have widely differing transcriptional profiles and can be delineated by differential expression of the neurogenic basic helix-loop-helix transcription factors *ASCL1* and *NEUROD1*, suggesting that primary SCLC can be found along the same spectrum of differentiation found in cell lines and PDXs.

Finally, we report striking overexpression of *EZH2* in primary SCLC compared to normal lung as well as other primary tumors from TCGA and cell lines from the CCLE. *EZH2* overexpression was correlated with increased promoter methylation across tumor types in TCGA. Various approaches to target *EZH2* are being explored including inhibition of the catalytic domain ([40]) and inhibition of protein-protein interactions to disrupt the PRC2 complex ([41]). We explored pharmacologic inhibition of EZH2 in SCLC and demonstrated that EPZ-6438 profoundly inhibited tumor growth *in vivo* in an SCLC PDX.

These data support further studies of the role that SCLC subtypes play in the clinical course of the disease. Given the exceptionally high level of promoter methylation observed in SCLC, new approaches to epigenetic targeting should be explored, inclusive of targeting EZH2.

Materials and Methods

Primary SCLC Samples

All clinical samples were extracted in a single batch using the Qiagen All-prep kit. All other samples were extracted from fresh-frozen pellets by the Hopkins Microarray and Deep Sequencing core facility. Aliquots of each sample were examined by agarose gel electrophoresis and spectrophotometry, and determined to be of good quality compared to a genomic DNA reference standard.

Methylation Beadchip Assay

Bisulfite conversion of DNA was carried out using the EZ DNA Methylation Kit (Zymo Research) according to manufacturer's instructions. Bisulfite-converted DNA was analyzed using Illumina's Infinium Human Methylation450 Beadchip Kit (WG-314-1001) according to the manufacturer's instructions. Each beadchip probes 485,577 CpG loci in the human genome. Polymer-coated chips were image-processed in Illumina's iScan scanner.

Data Acquisition

Raw .idat files were imported using the Bioconductor suite for R. Methylation levels, β, were represented according to the following equation:

$$\beta = \frac{M}{M + U + 100}$$

Where M represents the signal intensity of the methylated probe, and U represents the signal intensity of the unmethylated probe. Illumina recommends adding the constant 100 to the denominator to regularize β-values with very low values for both M and U. Probe dye bias was normalized using built-in control probes. Data points with a detection p value of <.01 were dropped. Finally, probes from X and Y chromosomes were excluded, leaving 473,864 unique probes.

Cluster Analysis

Principal component analysis was performed on quantile normalized data, excluding normal lung samples. Informative probes with a standard deviation >.2 were used for Consensus Clustering of Ilumina 450k data. Different clustering algorithms and number of clusters were investigated extensively including k-means, PAM, and hierarchical clustering approaches. The solution with the number of clusters reported here is based on cluster stability, silhouette width, the change in the area under the cumulative distribution function (ΔCDF), and biological significance of predicted subtypes. Scatter plots comparing methylation between two groups represent the average β-value at each probe for that group with color values indicating density after two-dimensional kernel density smoothing.

Differential Methylation and Gene Expression

The difference in DNA methylation β-value was taken between each primary SCLC sample and its patient-matched normal lung. A linear model was fit to the remaining probes and p-values were calculated and adjusted by the method of Bonferroni. A q-value cutoff of .05 was used, resulting in 1,689 significantly differentially methylated CpG sites. Differentially methylated regions (DMRs) were identified as previously described ([23]). For gene expression analysis, RNA-seq counts were converted to log2 counts per million and correlated by the Spearman method to β-values of differentially methylated CpGs. Concordance at the top (CAT) plots were generated by comparing the concordance between different contrasts at the top of the list of differentially methylated probes as a function of the size of the ranked probe list.

Patient-derived xenografts

PDXs were propagated as previously described with the addition of a dissociation step using a gentleMACS automated dissociator and mouse tissue dissociation kit (Miltenyi) prior to resuspension in 50% matrigel in HBSS ([20]). LX lines were derived at Johns Hopkins University. Lu lines were obtained from Stem CentRx, Inc (San Francisco, CA). PDX identity was confirmed by Short Tandem Repeat analysis using the PowerPlex 18 panel (Promega; DDC Medical). The LX92 PDX model was engrafted from fresh tumor tissue in

6–8 week old female athymic mice (Hsd:Athymic-Nude:*Foxn1*^{nu}). Briefly, 5×10^6 viable cells/mouse were injected subcutaneous into the right hind flank in a 1:1 mix of HBSS and matrigel basement membrane (Corning) as a final volume of 100 μL. Mice were randomized to treatment arms once tumors reached ~150 mm^3. EPZ-6438 was purchased from ActiveBiochem and formulated in 0.5% NaCMC w/ 0.1% Tween-80 in water. Twice-daily (BID) dosing was done on a 10AM/4PM schedule, Mon-Fri. Tumor volumes and mice weights were measured twice weekly. Tumor tissues used for western blot were collected 2 hours after the final dose.

Ex vivo cell culture

PDXs were dissociated as above. Single cell suspensions were filtered through 70 μm mesh, washed twice with wash buffer (PBS, 2% FBS and 1 mM EDTA) and red blood cells were lysed with ACK buffer (Crystalgen Inc.). Approximately 1×10^6 viable cells were seeded in 10 mL of DMEM:F12 supplemented with a EGM-2 SingleQuot growth factor kit (Lonza). Once cultures were established (~72 hours post-dissociation), 96-well plates were seeded with 5,000 cells/well in 100uL of ex vivo culture media and the following compounds were administered daily to a final concentration of 1uM: DMSO (vehicle), EPZ-5687, GSK343 or UNC1999 (Selleck Chemicals). Resazurin conversion of alamarBlue® (Invitrogen) was monitored on a compatible plate reader (Synergy Neo HTS; BioTek)

Western blotting

Protein was extracted using RIPA buffer supplemented with Halt™ protease and phosphatase inhibitor cocktails (Pierce). Extraction of nuclear proteins required 3 sequential 5-second pulses at 65% amplitude using a 120 W needle-tip ultrasonic processor (Fisher Scientific). The following antibodies were used for western blot according to the manufacturer's recommendations: EZH1 (Thermo; #PA1-41114), EZH2 (Cell Signaling; #5246), β-actin (Cell Signaling; #4967), H3K27me2 (Cell Signaling; #9728), H3K27me3 (Cell Signaling; #9733) and total H3 (Cell Signaling; #4499).

Public Data

RNAseq, copy number variation and mutation data are previously described and available at the European Genome-phenome Archive (EGAS00001000334) ([7]). TCGA samples used for this study are listed in Supplementary Table S8.

Supplementary Material

Refer to Web version on PubMed Central for supplementary material.

Acknowledgements

We thank Inna Kodos in the Sloan Kettering Antitumor Assessment Core for her technical expertise. We are grateful to all members of the Rudin and Hann labs for thoughtful discussions.

Financial support: SU2C, P30 CA008748

References

1. Siegel R, Naishadham D, Jemal A. Cancer statistics, (2012). CA Cancer J Clin. 2012; 62:10–29. [PubMed: 22237781]
2. Jemal A, Bray F, Center MM, Ferlay J, Ward E, Forman D. Global cancer statistics. CA Cancer J Clin. 2011; 61:69–90. [PubMed: 21296855]
3. Wistuba II, Gazdar AF, Minna JD. Molecular genetics of small cell lung carcinoma. Semin Oncol. 2001; 28:3–13. [PubMed: 11479891]
4. Oze I, Hotta K, Kiura K, Ochi N, Takigawa N, Fujiwara Y, et al. Twenty-seven years of phase III trials for patients with extensive disease small-cell lung cancer: disappointing results. PLoS ONE. 2009; 4:e7835. [PubMed: 19915681]
5. Madrigal PA, Manga GP, Palomero I, Gomez RG. VP16-213 combined with cis-platinum (CDDP) in the treatment of small cell carcinoma of the lung (SCLC). Cancer Chemother Pharmacol. 1982; 7:203–204. [PubMed: 6282485]
6. Lara PN Jr, Natale R, Crowley J, Lenz HJ, Redman MW, Carleton JE, et al. Phase III trial of irinotecan/cisplatin compared with etoposide/cisplatin in extensive-stage small-cell lung cancer: clinical and pharmacogenomic results from SWOG S0124. J Clin Oncol. 2009; 27:2530–2535. [PubMed: 19349543]
7. Rudin CM, Durinck S, Stawiski EW, Poirier JT, Modrusan Z, Shames DS, et al. Comprehensive genomic analysis identifies SOX2 as a frequently amplified gene in small-cell lung cancer. Nature Genet. 2012; 44:1111–1116. [PubMed: 22941189]
8. Peifer M, Fernandez-Cuesta L, Sos ML, George J, Seidel D, Kasper LH, et al. Integrative genome analyses identify key somatic driver mutations of small-cell lung cancer. Nat Genet. 2012; 44:1104–1110. [PubMed: 22941188]
9. Clinical Lung Cancer Genome P, Network Genomic M. A genomics-based classification of human lung tumors. Science Transl Med. 2013; 5:209ra153.
10. Cancer Genome Atlas Research N. Comprehensive genomic characterization of squamous cell lung cancers. Nature. 2012; 489:519–525. [PubMed: 22960745]
11. Cancer Genome Atlas N. Comprehensive molecular characterization of human colon and rectal cancer. Nature. 2012; 487:330–337. [PubMed: 22810696]
12. Cancer Genome Atlas N. Comprehensive molecular portraits of human breast tumours. Nature. 2012; 490:61–70. [PubMed: 23000897]
13. Cancer Genome Atlas Research N. Comprehensive genomic characterization defines human glioblastoma genes and core pathways. Nature. 2008; 455:1061–1068. [PubMed: 18772890]
14. Kalari S, Jung M, Kernstine KH, Takahashi T, Pfeifer GP. The DNA methylation landscape of small cell lung cancer suggests a differentiation defect of neuroendocrine cells. Oncogene. 2013; 32:3559–3568. [PubMed: 22907430]
15. Rauch T, Pfeifer GP. Methylated-CpG island recovery assay: a new technique for the rapid detection of methylated-CpG islands in cancer. Lab Invest. 2005; 85:1172–1180. [PubMed: 16025148]
16. Hann CL, Rudin CM. Fast, hungry and unstable: finding the Achilles' heel of small-cell lung cancer. Trends Mol Med. 2007; 13:150–157. [PubMed: 17324626]
17. Hansen KD, Timp W, Bravo HC, Sabunciyan S, Langmead B, McDonald OG, et al. Increased methylation variation in epigenetic domains across cancer types. Nature Genet. 2011; 43:768–775. [PubMed: 21706001]
18. Poirier JT, Dobromilskaya I, Moriarty WF, Peacock CD, Hann CL, Rudin CM. Selective tropism of Seneca Valley virus for variant subtype small cell lung cancer. J Natl Cancer Instit. 2013; 105:1059–1065.
19. Carney DN, Gazdar AF, Bepler G, Guccion JG, Marangos PJ, Moody TW, et al. Establishment and identification of small cell lung cancer cell lines having classic and variant features. Cancer Res. 1985; 45:2913–2923. [PubMed: 2985257]
20. Daniel VC, Marchionni L, Hierman JS, Rhodes JT, Devereux WL, Rudin CM, et al. A primary xenograft model of small-cell lung cancer reveals irreversible changes in gene expression imposed by culture in vitro. Cancer Res. 2009; 69:3364–3373. [PubMed: 19351829]

21. Irizarry RA, Warren D, Spencer F, Kim IF, Biswal S, Frank BC, et al. Multiple-laboratory comparison of microarray platforms. Nature Methods. 2005; 2:345–350. [PubMed: 15846361]
22. Berman BP, Weisenberger DJ, Aman JF, Hinoue T, Ramjan Z, Liu Y, et al. Regions of focal DNA hypermethylation and long-range hypomethylation in colorectal cancer coincide with nuclear lamina-associated domains. Nature Genet. 2012; 44:40–46. [PubMed: 22120008]
23. Jaffe AE, Murakami P, Lee H, Leek JT, Fallin MD, Feinberg AP, et al. Bump hunting to identify differentially methylated regions in epigenetic epidemiology studies. Int J Epidemiol. 2012; 41:200–209. [PubMed: 22422453]
24. Gardner EE, Connis N, Poirier JT, Cope L, Dobromilskaya I, Gallia GL, et al. Rapamycin rescues ABT-737 efficacy in small cell lung cancer. Cancer Res. 2014; 74:2846–2856. [PubMed: 24614082]
25. Smith LT, Lin M, Brena RM, Lang JC, Schuller DE, Otterson GA, et al. Epigenetic regulation of the tumor suppressor gene TCF21 on 6q23-q24 in lung and head and neck cancer. Proc Natl Acad Sci USA. 2006; 103:982–987. [PubMed: 16415157]
26. Wilkerson MD, Yin X, Hoadley KA, Liu Y, Hayward MC, Cabanski CR, et al. Lung squamous cell carcinoma mRNA expression subtypes are reproducible, clinically important, and correspond to normal cell types. Clin Cancer Res. 2010; 16:4864–4875. [PubMed: 20643781]
27. Mack SC, Witt H, Piro RM, Gu L, Zuyderduyn S, Stutz AM, et al. Epigenomic alterations define lethal CIMP-positive ependymomas of infancy. Nature. 2014; 506:445–450. [PubMed: 24553142]
28. Zouridis H, Deng N, Ivanova T, Zhu Y, Wong B, Huang D, et al. Methylation subtypes and large-scale epigenetic alterations in gastric cancer. Science Transl Med. 2012; 4:156ra40.
29. Noushmehr H, Weisenberger DJ, Diefes K, Phillips HS, Pujara K, Berman BP, et al. Identification of a CpG island methylator phenotype that defines a distinct subgroup of glioma. Cancer Cell. 2010; 17:510–522. [PubMed: 20399149]
30. Weisenberger DJ, Siegmund KD, Campan M, Young J, Long TI, Faasse MA, et al. CpG island methylator phenotype underlies sporadic microsatellite instability and is tightly associated with BRAF mutation in colorectal cancer. Nature Genet. 2006; 38:787–793. [PubMed: 16804544]
31. Bady P, Sciuscio D, Diserens AC, Bloch J, van den Bent MJ, Marosi C, et al. MGMT methylation analysis of glioblastoma on the Infinium methylation BeadChip identifies two distinct CpG regions associated with gene silencing and outcome, yielding a prediction model for comparisons across datasets, tumor grades, and CIMP-status. Acta Neuropath. 2012; 124:547–560. [PubMed: 22810491]
32. Chang CJ, Hung MC. The role of EZH2 in tumour progression. Brit J Cancer. 2012; 106:243–247. [PubMed: 22187039]
33. Bracken AP, Pasini D, Capra M, Prosperini E, Colli E, Helin K. EZH2 is downstream of the pRB-E2F pathway, essential for proliferation and amplified in cancer. EMBO. 2003; 22:5323–5335.
34. Vogelstein B, Papadopoulos N, Velculescu VE, Zhou S, Diaz LA Jr, Kinzler KW. Cancer genome landscapes. Science. 2013; 339:1546–1558. [PubMed: 23539594]
35. Byers LA, Wang J, Nilsson MB, Fujimoto J, Saintigny P, Yordy J, et al. Proteomic profiling identifies dysregulated pathways in small cell lung cancer and novel therapeutic targets including PARP1. Cancer Discov. 2012; 2:798–811. [PubMed: 22961666]
36. Ziller MJ, Gu H, Muller F, Donaghey J, Tsai LT, Kohlbacher O, et al. Charting a dynamic DNA methylation landscape of the human genome. Nature. 2013; 500:477–481. [PubMed: 23925113]
37. Varley KE, Gertz J, Bowling KM, Parker SL, Reddy TE, Pauli-Behn F, et al. Dynamic DNA methylation across diverse human cell lines and tissues. Genome Res. 2013; 23:555–567. [PubMed: 23325432]
38. Wilkerson MD, Yin X, Walter V, Zhao N, Cabanski CR, Hayward MC, et al. Differential pathogenesis of lung adenocarcinoma subtypes involving sequence mutations, copy number, chromosomal instability, and methylation. PloS One. 2012; 7:e36530. [PubMed: 22590557]
39. Meuwissen R, Linn SC, Linnoila RI, Zevenhoven J, Mooi WJ, Berns A. Induction of small cell lung cancer by somatic inactivation of both Trp53 and Rb1 in a conditional mouse model. Cancer Cell. 2003; 4:181–189. [PubMed: 14522252]

40. Wee ZN, Li Z, Lee PL, Lee ST, Lim YP, Yu Q. EZH2-Mediated Inactivation of IFN-gamma-JAK-STAT1 Signaling Is an Effective Therapeutic Target in MYC-Driven Prostate Cancer. Cell Rep. 2014; 8:204–216. [PubMed: 24953652]

41. Kim W, Bird GH, Neff T, Guo G, Kerenyi MA, Walensky LD, et al. Targeted disruption of the EZH2-EED complex inhibits EZH2-dependent cancer. Nature Chem Biol. 2013; 9:643–650. [PubMed: 23974116]

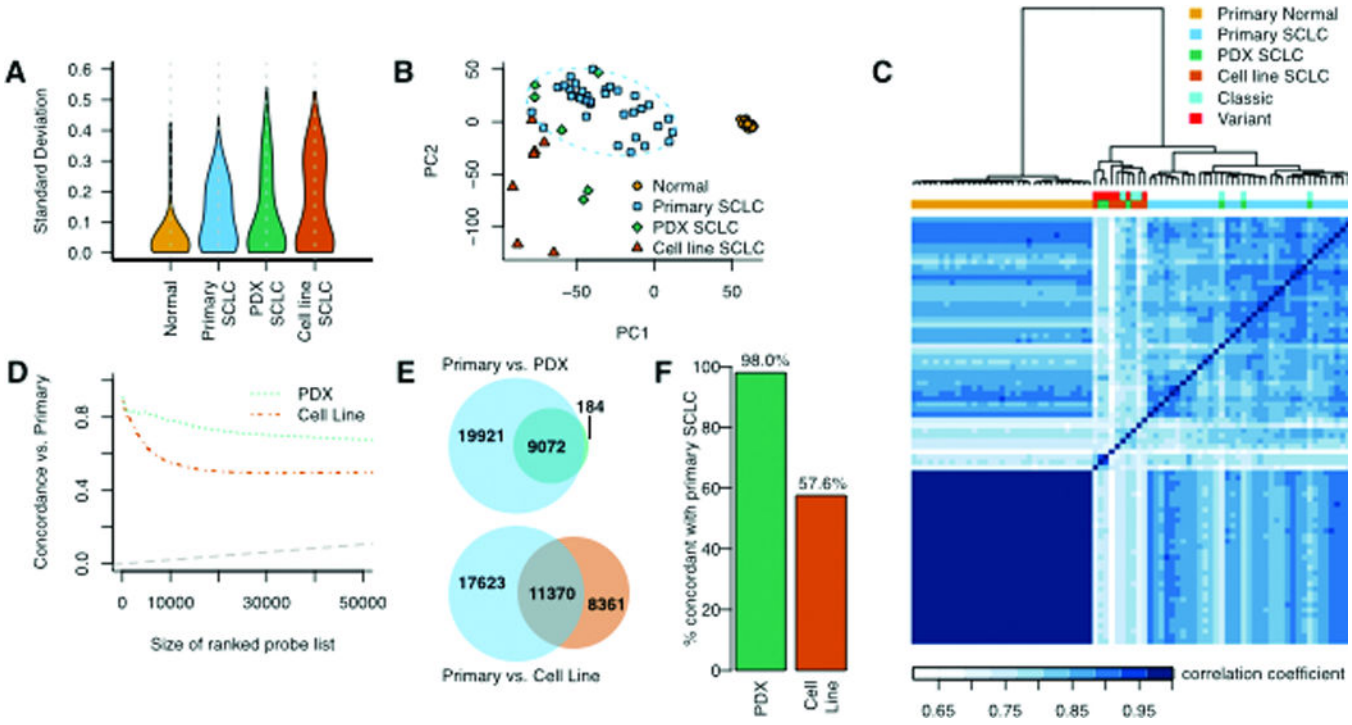

Figure 1. DNA methylation patterns in normal lung, primary SCLC, PDXs and cell lines

A) Violin plot of CpG β-value standard deviations for each sample type demonstrate that tissue-specific methylation in primary normal samples is consistent between patients while cancer samples can have a long tail of high variation. **B**) Principal component analysis demonstrates clustering of 4/6 PDXs with primary SCLC. Cell lines can be distinguished from all other samples using just two principal components. **C)** Hierarchical clustering of Spearman correlation coefficients between all samples. **D)** Concordance at the top (CAT) plot demonstrates that concordance with primary SCLC is consistent for PDXs while cell lines rapidly lose concordance as the size of the ranked gene list considered increases. **E–F)** PDXs have 98% concordance of differentially expressed genes (*q*-value cutoff 1×10^{6}), while cell lines exhibit epigenetic changes associated with long-term culture.

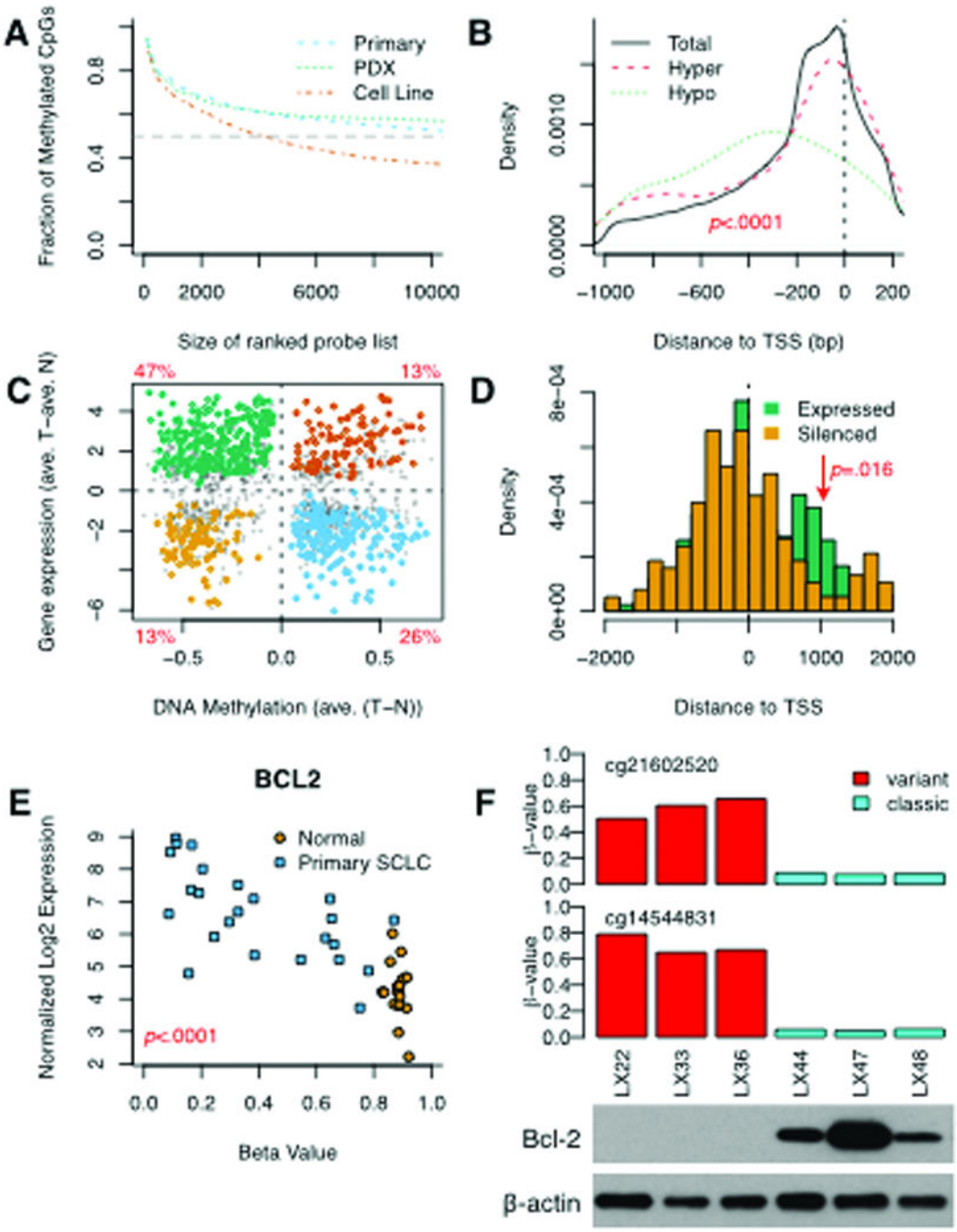

Figure 2. Characteristics of differential methylation between SCLC and normal lung

A) CpG methylation versus normal lung in each group decreases as a function of the size of the ranked gene list considered increases, indicating that the majority of significant differences are methylation events. **B)** CpGs hypermethylated in SCLC are more likely to be located immediately upstream of the TSS or within the first exon than hypomethylated CpGs, which are distributed more evenly throughout the promoter region ($p<.0001$, two-tailed Wilcoxon rank sum test). **C)** CpG methylation is predominantly negatively correlated with gene expression, comprising 73% of differentially methylated CpGs. **D)**

Hypomethylated CpGs that are associated with gene expression are significantly more likely to be found in gene bodies than are hypomethylated CpGs associated with silencing (p=.016, two-tailed Wilcoxon rank sum test). **E)** Methylation in the first exon of *BCL2* is strongly correlated with gene expression silencing. *BCL2* methylation may be one mechanism by which some SCLC tumors lack expression of *BCL2* (p<.0001, Spearman correlation test). **F)** *BCL2* methylation in SCLC PDXs is strongly associated with silencing of Bcl-2 protein expression in variant subtype models as measured by Western blot.

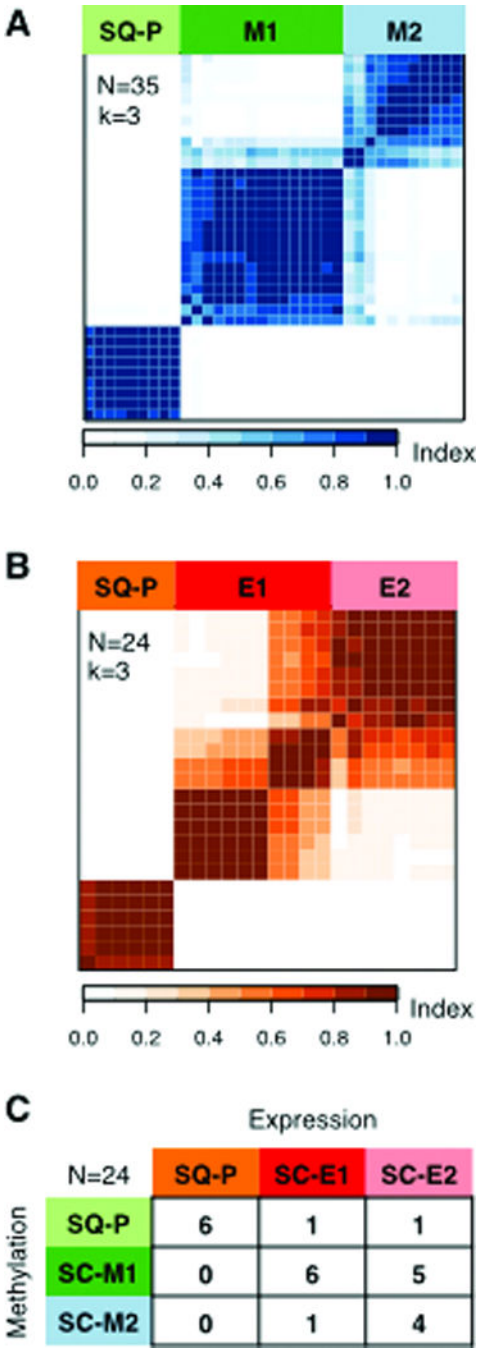

Figure 3. Identification of SCLC subtypes by consensus clustering

A) Consensus clustering of DNA methylation reveals 3 distinct groups of SCLC DNA methylation. Two groups we designate here as SC-M1 and SC-M2, while a third group closely resembles primitive squamous cell tumors previously designated as SQ-P. **B)** Consensus clustering of RNA-seq gene expression also revealed a stable cluster consistent with primitive squamous cell tumors as well as two larger clusters with a less distinct consensus. **C)** 6/6 tumors in the gene expression SQ-P group belong to the identical

methylation cluster. The other subtypes are less clearly distinguished exclusively by gene expression.

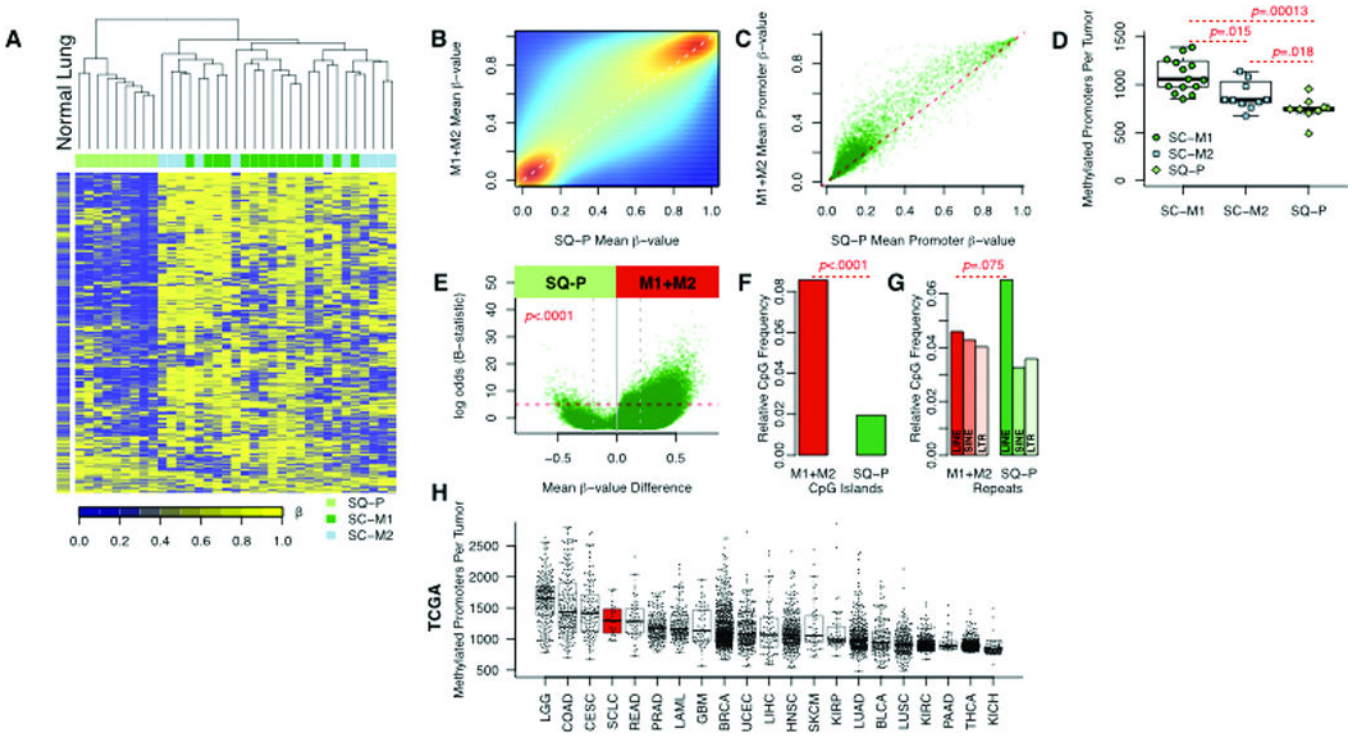

Figure 4. SCLC promoter methylation is higher in the SC-M1 and SC-M2 subgroups than in the SQ-P primitive squamous like subtype or the majority of tumors in TCGA

A) Unsupervised clustering of the most highly variable CpGs was consistent with consensus clustering approaches. The SCLC subtypes M1 and M2 had consistently higher DNA methylation. **B)** Genome-wide CpG methylation is consistently higher in SCLC M1+M2 than SQ-P. **C)** Average DNA methylation within promoters is also lower in SQ-P. **D)** The number of methylated promoters in each sample is significantly lower in the SQ-P subtype than in other SCLC subtypes (Wilcoxon rank sum test) **E)** Global CpG methylation levels are consistently lower in SQ-P than other subtypes of SCLC (binomial distribution test). **F) and G)** Of the significantly differentially methylated CpGs between SQ-P vs. other SCLC, the frequency of methylated CpGs in CpG island containing promoters is significantly lower in SQ-P (proportionality test) while there is a trend of increased methylation in repetitive elements in SQ-P that fails to reach statistical significance. **H)** Average methylation in CpG island-containing promoters in SCLC is among the highest of any tumors in TCGA, including tumor types with defined genetic mechanisms for genome-wide hypermethylation.

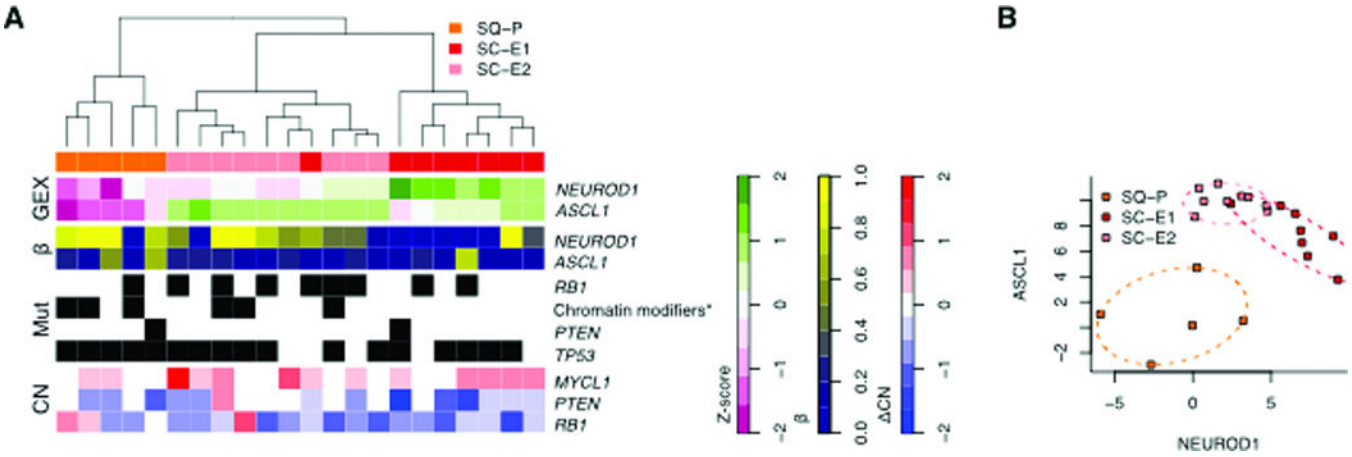

Figure 5. Differentially expressed genes among SCLC subtypes

A) Differentially expressed genes between the different subgroup indicate distinct differences in neuroendocrine differentiation. Despite the distinct epigenetic subtypes observed in this study, mutation and copy loss of *RB1*, a hallmark genetic lesion of SCLC, is nearly universal including within the group of primitive squamous-like tumors. **B)** Among the top differentially expressed genes are *ASCL1* and *NEUROD1*, which we have previously identified in patient derived xenografts as important classifiers.

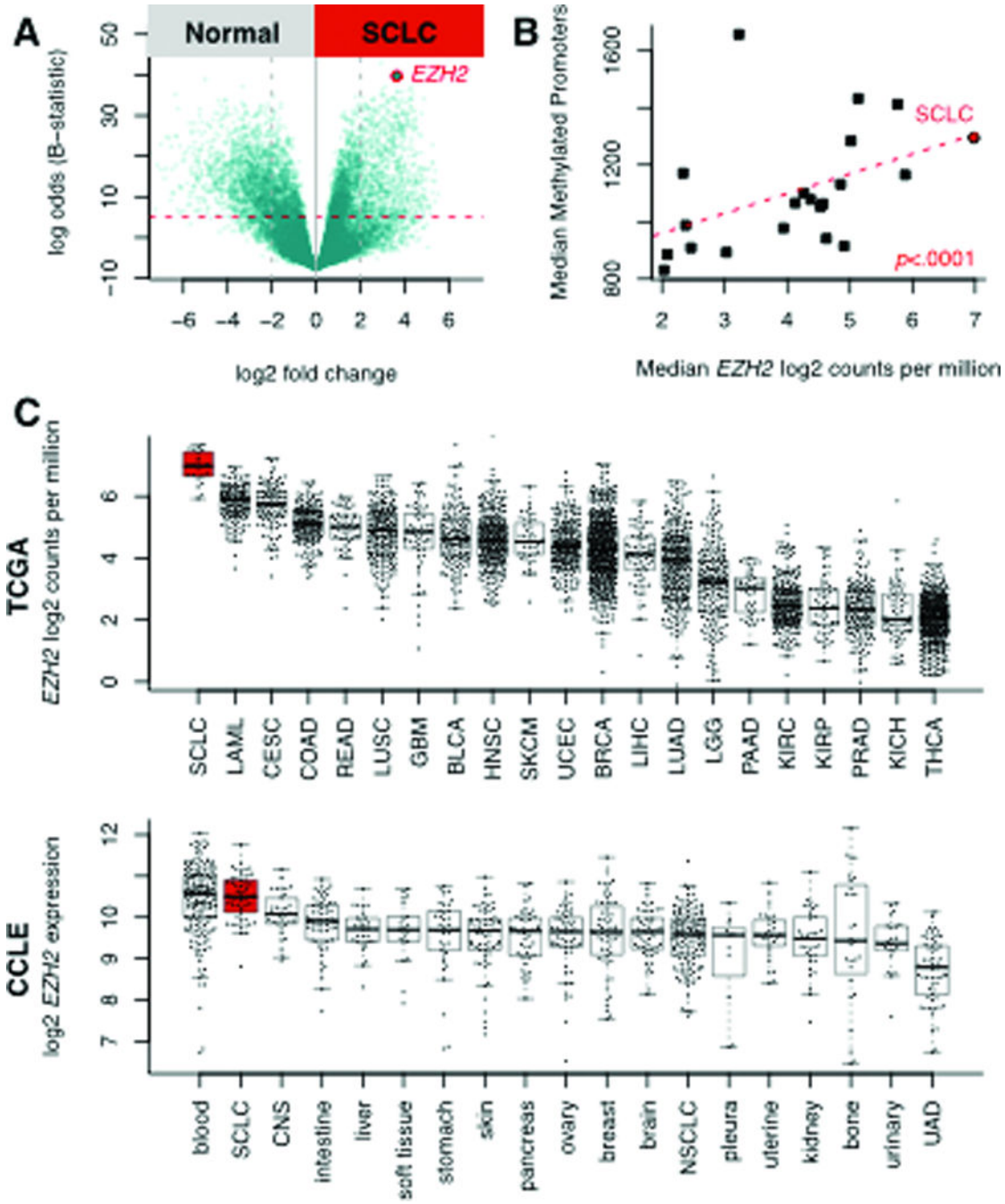

Figure 6. EZH2 is among the most significantly differentially expressed genes in SCLC compared to normal lung or other tumor types in TCGA

A) *EZH2* is the second most significantly differentially expressed gene when compared to normal lung control with >12-fold higher expression levels. **B)** Median expression levels of *EZH2* are significantly correlated with high levels of promoter methylation in SCLC and TCGA data sets (Spearman's rho test of correlation). **C)** *EZH2* gene expression in SCLC is higher than any other TCGA tumor set and among the highest of any tumor type in the cell lines found in the CCLE.

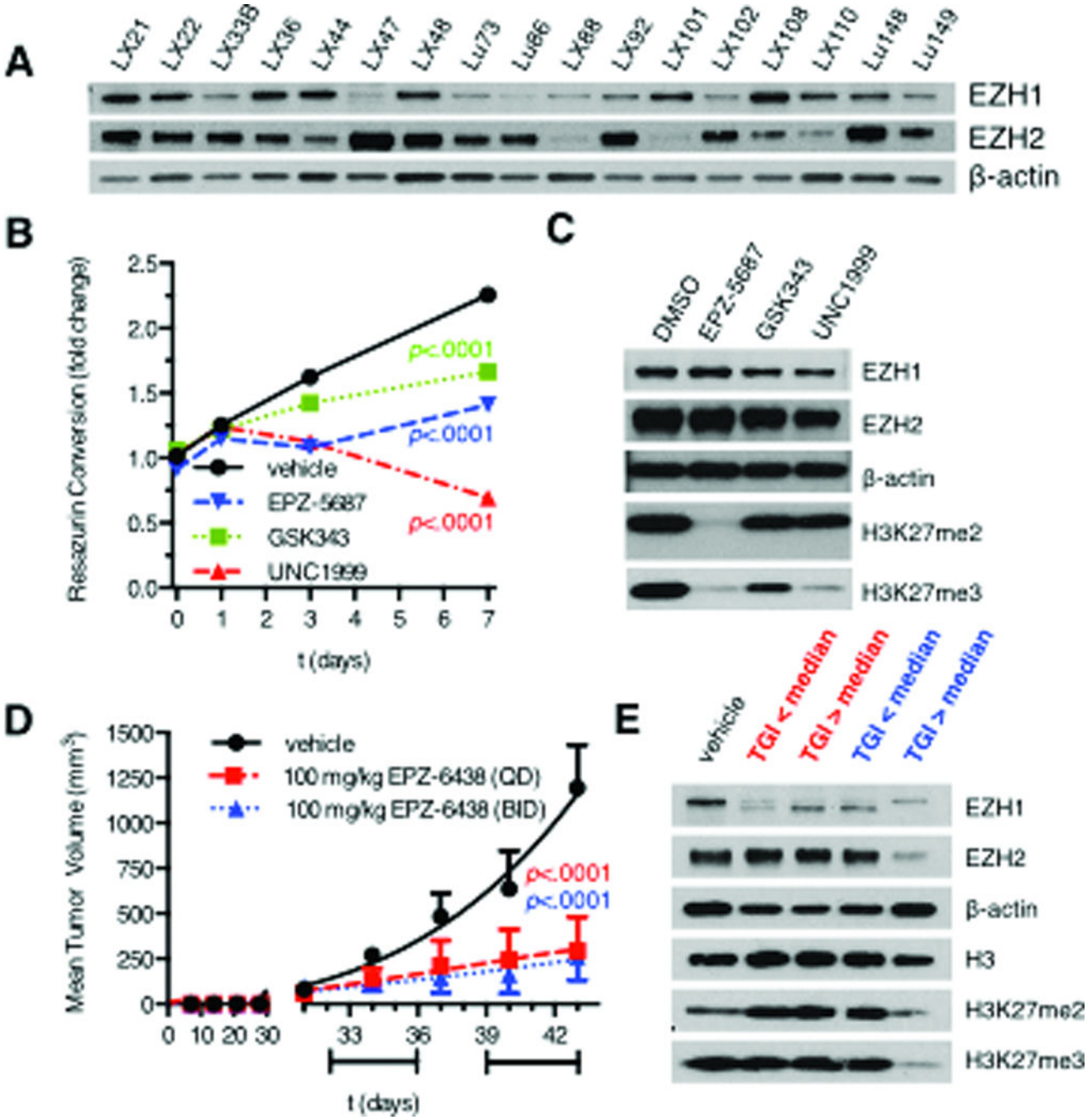

Figure 7. Pharmacologic inhibition of EZH2 *in SCLC inhibits growth in vitro* and *in vivo*

A) EZH1 and EZH2 are consistently expressed in a panel of SCLC PDXs as measured by Western blot **B)** *Ex vivo* growth of the SCLC PDX LX92 is significantly inhibited by the EZH2 inhibitors EPZ-5687, GSK343, and UNC1999 as measured by resazurin conversion (2-way ANOVA, adjusted for multiple comparisons by the method of Dunnet) **C)** Western blot analysis of day 7 lysates from LX92 lysates treated with various EZH2 inhibitors. **D)** *In vivo* growth of the SCLC PDX LX92 is significantly inhibited by the EZH2 inhibitor EPZ-6438. **E)** Western blot analysis of endpoint LX92 tumor lysates treated with various

EPZ-6438 treatment schedules. Tumors with growth inhibition greater than the median (TGI>median) for each treatment group were pooled separately from those with less robust response (TGI<median) to assess correlation between TGI and pharmacodynamic response.